Journal of Applied Physics

RESEARCH ARTICLE | JULY 18 2024

Thermodynamic properties of $R_2Fe_{14}B$ (R=Dy, Nd) and dysprosium random substitution effect on coercivity in neodymium permanent magnets

Masamichi Nishino ; Hiroshi Hayasaka ; Seiji Miyashita

J. Appl. Phys. 136, 033904 (2024)
https://doi.org/10.1063/5.0217917

AIP Publishing

Journal of Applied Physics ARTICLE pubs.aip.org/aip/jap

Thermodynamic properties of $R_2Fe_{14}B$ (R=Dy, Nd) and dysprosium random substitution effect on coercivity in neodymium permanent magnets

Cite as: J. Appl. Phys. **136**, 033904 (2024); doi: 10.1063/5.0217917
Submitted: 7 May 2024 · Accepted: 25 June 2024 ·
Published Online: 18 July 2024

Masamichi Nishino,[1,a)] Hiroshi Hayasaka,[1,2] and Seiji Miyashita[3,4]

AFFILIATIONS

[1]Research Center for Materials Nanoarchitectonics, National Institute for Materials Science, 1-1 Namiki, Tsukuba, Ibaraki 305-0044, Japan
[2]Global Research and Development Center for Business by Quantum-AI technology, National Institute of Advanced Industrial Science and Technology, 1-1-1, Umezono, Tsukuba, Ibaraki 305-8568, Japan
[3]JSR-UTokyo Collaboration Hub, CURIE, Department of Physics, The University of Tokyo, 7-3-1 Hongo, Tokyo 113-0033, Japan
[4]The Physical Society of Japan, 2-31-22 Yushima, Tokyo 113-0033, Japan

[a)]**Author to whom correspondence should be addressed:** nishino.masamichi@nims.go.jp

ABSTRACT

Neodymium (Nd) magnets ($Nd_2Fe_{14}B$) are key materials for achieving high energy conversion efficiency. The coercive forces (fields) of the magnets are often reinforced by adding dysprosium (Dy), especially at high temperatures. To understand the magnetic properties of Dy-substituted systems $(Nd_{1-x}Dy_x)_2Fe_{14}B$, it is important to study those of $Dy_2Fe_{14}B$ and $Nd_2Fe_{14}B$ and analyze the difference in detail from a microscopic viewpoint. Applying a recently developed atomistic model approach, we investigated thermodynamic properties of these magnets. We studied the temperature and field dependences of the magnetizations, and anisotropy fields and energies. We found that the simulation results captured the characteristic features of the experimentally observed data. We discuss the detail with the magnetization profiles of the component atoms. Furthermore, we investigated the effect of Dy random substitution on the coercivity in two systems: one in contact with vacuum and the other in contact with a grain boundary phase. We found that the threshold fields increased almost linearly with the concentration of Dy atoms in both systems, which was compared to the results of the layer-by-layer substitution effect analyzed in our previous work. We discuss the influence of the arrangement of Dy atoms on coercivity enhancement.

I. INTRODUCTION

Control of the coercivity of permanent magnets and realization of higher coercivity at higher temperatures is an important issue for achieving high energy conversion efficiency. Coercivity is a nonequilibrium property that depends on various factors such as grain boundary properties.[1–9] Therefore, understanding the mechanism of coercivity remains challenging.

Neodymium (Nd) magnets ($Nd_2Fe_{14}B$[10–19]), known as powerful permanent magnets with high coercivity, are key materials for achieving high energy conversion efficiency. They are used in motors, generators, electrical appliances, and other applications.[20] The use of Nd magnets is expected to increase in the future, partly because of the growing demand for electric vehicle (EV) motors. Studies on the coercivity mechanism of Nd magnets and attempts to achieve higher coercivity at higher temperatures have become increasingly significant.

Neodymium magnets have a problem with coercivity at high temperatures, and the coercivity of the magnets is often reinforced by adding dysprosium (Dy). The formation of Dy-rich shells, $(Nd_{1-x}Dy_x)_2Fe_{14}B$, is considered important for the reinforcement of the coercivity. Experiments using the grain boundary diffusion method have shown that the coercivity increases without losing remanence,[21–25] and the formation of a Dy-rich shell between the grain boundary and core grain has been observed.[25] The coercivity

enhancement effect of the Dy-rich shell was also pointed out in coarse-grained micromagnetics model studies with macroscopic parameters of the Dy-substituted phase.[26,27]

Micromagnetics continuum modeling of permanent magnets has been applied to the analysis of magnetic properties.[28] This method has the advantage of being able to treat large systems and has had some success in analyzing qualitative aspects of magnetization reversals. However, because of the coarse graining and application of macroscopic magnetic parameters, the microscopic details of crystal structures and magnetic parameters are ignored. In addition, as investigated in Ref. 29, it is difficult, in principle, to treat accurately temperature effects and thermal fluctuations in coarse-grained continuum modeling.

The temperature effects of $R_2Fe_{14}B$ have been studied by the mean-field approximation,[30,31] but the mean-field approximation neglects thermal fluctuations. Thus, it is not sufficient to study accurate thermodynamic properties and often leads to serious misinterpretation. For example, in the $S = 1$ simple Heisenberg model with the magnetic interaction J on a simple cubic lattice (six nearest neighbors), the mean-field theory leads to the critical temperature ($2J$) around 40% higher than the exact value ($1.44J$) obtained by treating the fluctuations.[32]

To study the microscopic details of magnetic properties at finite temperatures, recently developed atomistic models are indispensable. In atomistic modeling, microscopic magnetic parameters, which reflect the lattice structure (Fig. 1), thermal fluctuations, and dynamics to realize the thermal equilibrium[33,34] can be treated appropriately. Atomistic model studies have elucidated the qualitative and quantitative properties of Nd magnets at zero and finite temperatures.[7,35–52]

Using an atomistic model approach, we recently studied the coercivity enhancement by Dy substitution into Nd magnets.[50] We found that the crystal electric field (CEF) energy barrier of Dy atoms was more resistant to temperature increase, which is considered to be an origin of the coercivity enhancement by Dy substitution, in addition to the difference in the magnetic interaction between rare-earth and iron atoms, that is, antiferromagnetic coupling between Dy and Fe moments while ferromagnetic coupling between Nd and Fe moments. We also found that an increase in the number of Dy-substituted layers (100% replacement of Nd by Dy) enhanced the coercivity, and the coercivity increase was nearly proportional to the number of substituted layers.

It is important to study $Dy_2Fe_{14}B$ and $Nd_2Fe_{14}B$ in detail and make clear the difference in magnetic properties by the atomistic model approaches toward a full understanding of the coercivity enhancement mechanism. So far, $Nd_2Fe_{14}B$ has been studied using atomistic models,[7,35–50,52] but $Dy_2Fe_{14}B$ has not been studied yet. In the present paper, we investigated for the first time the thermodynamic properties of $Dy_2Fe_{14}B$ using an atomistic model approach and compared them with those of $Nd_2Fe_{14}B$. We found a satisfactory agreement with experimental observations. We discussed the detailed features of these magnets.

Second, we studied the Dy substitution effect. In our previous study (Ref. 50), we investigated the effect of Dy layer-by-layer substitution on the coercivity. In the present paper, we analyzed the effect of Dy random substitution on magnetization reversal in neodymium permanent magnets and compared the results with those of the previous study.

The rest of the paper is organized as follows. In Sec. II, the atomistic model is presented. In Sec. III, the methods for investigating static and dynamical properties are explained. In Sec. IV A, thermodynamic properties of $R_2Fe_{14}B$ (R=Dy, Nd) are studied. In Sec. IV B, the effect of Dy random substitution on magnetization reversal in neodymium permanent magnets is investigated. Section V is devoted to summary.

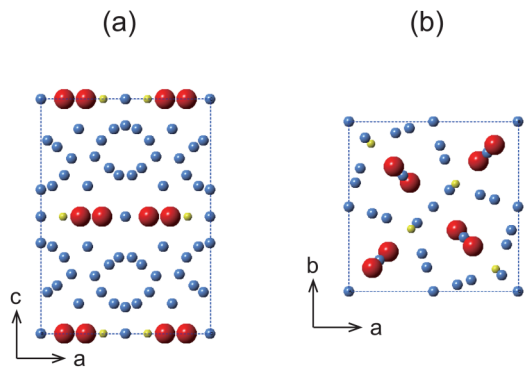

FIG. 1. (a) Side view and (b) top view of the unit cell of $R_2Fe_{14}B$. R denotes a rare-earth atom (Nd or Dy). In $Nd_2Fe_{14}B$, $l_a = l_b = 8.80$ Å, and $l_c = 12.20$ Å. In $Dy_2Fe_{14}B$, $l_a = l_b = 8.76$ Å, and $l_c = 12.01$ Å.

II. MODEL

The following atomistic Hamiltonian was adopted:

$$\mathcal{H} = -\sum_{i<j} 2J_{ij}\boldsymbol{s}_i \cdot \boldsymbol{s}_j - \sum_{i}^{\mathrm{Fe}} D_i(s_i^z)^2 + \sum_{i}^{\mathrm{R}} \sum_{l,m} \Theta_{l,i} A_{l,i}^m \langle r^l \rangle_i \hat{O}_{l,i}^m - h_x \sum_i S_i^x - h_z \sum_i S_i^z. \quad (1)$$

The first term denotes the exchange interaction J_{ij} between the ith and jth atoms (spins). The second term refers to the anisotropy energy of Fe atoms, and D_i is the anisotropy constant for the ith Fe atom. The third term represents the crystal electric field (CEF) energy of rare-earth atoms (Nd and/or Dy). The origin of this term is the electrostatic interaction between f electrons of rare-earth atoms and surrounding ions. This term plays an important role in magnetic properties of rare-earth magnets.[53] Here, $\Theta_{l,i}$, $A_{l,i}^m$, $\langle r^l \rangle_i$, and $\hat{O}_{l,i}^m$ are the Stevens factor, coefficient of the spherical harmonics of the crystalline electric field, an average of r^l over the radial wave function, and Stevens operator, respectively. In the fourth and fifth terms, h_x and h_z are the external fields applied in the x and z directions parallel to the a and c axes, respectively. We consider $l = 2, 4, 6$ and $m = 0$ (diagonal operators), which have the dominant contribution.

For Fe and B atoms, $\boldsymbol{s}_i$ denotes the magnetic moment at the ith site, while for Nd and Dy atoms, it is the moment of the valence (5d and 6s) electrons and is strongly coupled to the

moment of the 4f electrons, $\mathcal{J}_i = g_T \boldsymbol{J}_i \mu_B$, where g_T is the Landé g-factor and $\boldsymbol{J}_i$ is the total angular momentum. Thus, the total moment of a rare-earth atom is $\boldsymbol{S}_i = \boldsymbol{s}_i + \mathcal{J}_i$. For Nd atoms, $J = \mathcal{L} - \mathcal{S} = 9/2$ and $g_T = 8/11$, where $\mathcal{L}$ is the orbital angular momentum and $\mathcal{S}$ is the spin angular momentum, while for Dy atoms, $J = \mathcal{L} + \mathcal{S} = 15/2$ and $g_T = 4/3$. For the Fe and B atoms, we define $\boldsymbol{S}_i = \boldsymbol{s}_i$. As shown in Ref. 50, $\boldsymbol{s}_i$ of a Nd (Dy) atom and $\boldsymbol{S}_i (= \boldsymbol{s}_i)$ of an Fe atom are coupled antiferromagnetically, but $\boldsymbol{S}_i$ of a Nd atom and that of an Fe atom are coupled ferromagnetically. In contrast, $\boldsymbol{S}_i$ of a Dy atom and that of an Fe atom are coupled antiferromagnetically. Following the previous paper,[50] we used the exchange interactions and magnetic moments estimated using the Korringa–Kohn–Rostoker (KKR) first-principles method, anisotropy constants for Fe atoms (six types) provided by Ref. 54, and A_l^m provided by Yamada *et al.*[55] for Nd and Dy atoms in $R_2Fe_{14}B$ with $\langle r^l \rangle$ estimated by Ref. 56.

The lattice constants are close between $Nd_2Fe_{14}B$ and $Dy_2Fe_{14}B$, and as we reported in Ref. 50, the exchange interactions estimated by the KKR first-principles computation between Nd and Fe in $Nd_2Fe_{14}B$ and those between Dy and Fe in $Dy_2Fe_{14}B$ were very close. This suggests that the effect of the local distortions produced by Dy substitution is small, and we do not consider this effect in Dy substitution.

III. METHOD

A. Thermodynamical properties

We used a Metropolis importance-sampling Monte Carlo (MC) method to study equilibrium magnetizations at finite temperatures. The per-site magnetizations M_z, M_x, M, and M_{xy} for the $R_2Fe_{14}B$ model were defined as

$$M_z(R_2Fe_{14}B) = \frac{1}{N}\left\langle \left| \sum_{i=1}^{N} S_i^z \right| \right\rangle, \tag{2}$$

$$M_x(R_2Fe_{14}B) = \frac{1}{N}\left\langle \left| \sum_{i=1}^{N} S_i^x \right| \right\rangle, \tag{3}$$

$$M(R_2Fe_{14}B) \tag{4}$$

$$= \frac{1}{N}\left\langle \sqrt{\left(\sum_{i=1}^{N} S_i^x\right)^2 + \left(\sum_{i=1}^{N} S_i^y\right)^2 + \left(\sum_{i=1}^{N} S_i^z\right)^2} \right\rangle, \tag{5}$$

and

$$M_{xy}(R_2Fe_{14}B) = \frac{1}{N}\left\langle \sqrt{\left(\sum_{i=1}^{N} S_i^x\right)^2 + \left(\sum_{i=1}^{N} S_i^y\right)^2} \right\rangle, \tag{6}$$

respectively. Here, N is the number of all atoms (all spins) in the $R_2Fe_{14}B$ model and $\langle\rangle$ denotes thermal average.

We also define the atom-specified (per-site) magnetizations for each atom species: R and Fe, (We computed the magnetization of boron (B) atoms, but the contribution was negligible.)

$$m_z(A) = \frac{1}{N_A}\left\langle \left| \sum_{i=1}^{N_A} S_i^z \right| \right\rangle \times \mathrm{sgn}\left(\sum_{i=1}^{N_A} S_i^z \right), \tag{7}$$

$$m_x(A) = \frac{1}{N_A}\left\langle \left| \sum_{i=1}^{N_A} S_i^x \right| \right\rangle \times \mathrm{sgn}\left(\sum_{i=1}^{N_A} S_i^x \right), \tag{8}$$

$$m_{xy}(A) = \frac{1}{N_A}\left\langle \sqrt{\left(\sum_{i=1}^{N_A} S_i^x\right)^2 + \left(\sum_{i=1}^{N_A} S_i^y\right)^2} \right\rangle, \tag{9}$$

$$m(A) = \frac{1}{N_A}\left\langle \sqrt{\left(\sum_{i=1}^{N_A} S_i^x\right)^2 + \left(\sum_{i=1}^{N_A} S_i^y\right)^2 + \left(\sum_{i=1}^{N_A} S_i^z\right)^2} \right\rangle, \tag{10}$$

where A denotes R or Fe and N_A is the number of atom A in the $R_2Fe_{14}B$ model.

We performed 200 000 Monte Carlo steps (MCSs) for equilibration and the following 400 000 MCSs for measurement for a system of $6 \times 6 \times 6$ unit cells with periodic boundary conditions.

B. Dynamical properties

To study the threshold values of the field for magnetization reversal in Dy-substituted Nd magnet systems, we applied the sLLG equation[33,34]

$$\frac{\mathrm{d}}{\mathrm{d}t}\boldsymbol{S}_i = -\frac{\gamma}{1+\alpha_i^2}\boldsymbol{S}_i \times \boldsymbol{h}_i^{\mathrm{eff}} - \frac{\alpha_i \gamma}{(1+\alpha_i^2)S_i}\boldsymbol{S}_i \times \left[\boldsymbol{S}_i \times \boldsymbol{h}_i^{\mathrm{eff}}\right]. \tag{11}$$

Here, γ is the electron gyromagnetic ratio and α_i is the damping factor.

At finite temperatures, magnetization reversal is a barrier-crossing process by virtue of thermal fluctuations, which occurs in a stochastic process. To treat the thermal effect, a noise field was introduced into the effective field on the ith as

$$\boldsymbol{h}_i^{\mathrm{eff}} = -\frac{\partial \mathcal{H}}{\partial \boldsymbol{S}_i} + \boldsymbol{\xi}_i(t). \tag{12}$$

Here, $\boldsymbol{\xi}_i(t) = (\xi_i^x, \xi_i^y, \xi_i^z)$ is the white Gaussian noise field, which has the following properties:

$$\langle \xi_i^\mu(t) \rangle = 0, \quad \langle \xi_i^\mu(t)\xi_j^\nu(s) \rangle = 2\mathcal{D}_i \delta_{ij}\delta_{\mu\nu}\delta(t-s). \tag{13}$$

Temperature T is described by the following relation (fluctuation–dissipation relation):

$$\mathcal{D}_i = \frac{\alpha_i k_B T}{\gamma S_i}. \tag{14}$$

We applied a kind of middle-point method[34] equivalent to the Heun method[33] for the numerical integration of the equation in

the Stratonovich interpretation. We set the time step to $\Delta t = 0.1$ fs and $\alpha_i = 0.1$.[49]

Under a reversed field parallel to the z (c) direction ($h_z \neq 0$ and $h_x = 0$), we observed the time evolution of the magnetization

$$\tilde{M}_z = \sum_i S_i^z \tag{15}$$

starting from an all-down-spin state. According to the previous study,[49] the threshold magnetic field was determined as follows. For a given value of h_z, we performed twelve simulations using different random number sequences to generate the noise field. We counted the number (N_s) of samples (simulations) in which magnetization reversal occurred. The threshold field was then defined as the middle point of the interval between the upper limit of the field for $N_s = 0$ and the lower limit of the field for $N_s = 12$. The error bars in the threshold field represent the interval region of the field. We set $t_{max} = 0.5$ ns (5×10^6 time steps).

In experiments, a coercive field is often defined as a field in which the metastable magnetic state has a lifetime of 1s, i.e., relaxation time of 1s. However, this is not practical for real-time simulations. Because the reversal time increases exponentially around the threshold field, the threshold fields estimated in this study provide approximate coercive fields.[42]

IV. RESULTS

A. Differences in thermodynamic properties between $R_2Fe_{14}B$ magnets (R=Nd, Dy)

In Fig. 2, the temperature dependences of M_z, M, and M_{xy} under zero field for $Dy_2Fe_{14}B$ are compared with those of $Nd_2Fe_{14}B$. We found that the critical temperature T_c of $Dy_2Fe_{14}B$ was almost the same as that of $Nd_2Fe_{14}B$ ($T_c \simeq 870$ K). This is primarily because the values of J_{ij} were similar for the two magnets as shown in Ref. 50. The simulated critical temperatures (T_c) of the magnets were a little overestimated compared to the experimental values ($\simeq 600$ K).[13,15,16] We use the temperature in the scaled form T/T_c for comparison with experimental data.

The temperature dependences of the magnetizations in $Dy_2Fe_{14}B$ captured the characteristic features of the experimentally observed ones.[15,16] When the temperature was reduced, $M_z(Dy_2Fe_{14}B)$ increased from T_c and reached the maximum value of $M_z \simeq 0.87\,\mu_B$ at $T \simeq 0.58T_c$ (experimentally, $M_z \simeq 0.85\,\mu_B$ at $T \simeq 0.66T_c$) and decreased gradually to 0 K. $M_z \simeq 0.59\,\mu_B$ per site at 0 K was an approximation of the experimental estimate $M_z \simeq 0.66\,\mu_B$ at 4.2 K.[16]

$Nd_2Fe_{14}B$ exhibited a spin-reorientation transition at $T_R \simeq 150$ K in experiments.[16–18,55] It was simulated accurately, yielding $2.0\,\mu_B$/site at $T_R \simeq 150$ K, which was close to an experimental value of, $2.1\,\mu_B$/site at $T = T_R$.[16] $Dy_2Fe_{14}B$ did not exhibit spin-reorientation transition and a smooth curve in M_z, owing to the anisotropy energy parallel to the c-direction at all temperatures.[50]

We examined the detailed features of magnetizations in each component of the magnets. In Fig. 3, the temperature dependences of m_z(Dy) and m_{xy}(Dy) under zero field for $Dy_2Fe_{14}B$ are compared to those of m_z(Nd) and m_{xy}(Nd) for $Nd_2Fe_{14}B$. In Fig. 4, the temperature dependences of m_z(Fe) and m_{xy}(Fe) in $Dy_2Fe_{14}B$ are compared to those in $Nd_2Fe_{14}B$. The total magnetic moments of Nd and Fe atoms were ferromagnetically coupled but those of Dy and Fe atoms were antiferromagnetically coupled (Fig. 1 in Ref. 50). Thus, m_z(Dy) increased in the negative direction with a large magnitude blow T_c. As the temperature was lowered, the m_z(Dy) curve exhibited a pattern of first concaving downward, then upwards, and finally downward again, culminating at $m_z \simeq -10.4, \mu_B$ at 0 K. However, m_z(Nd) increased in the positive direction, and the growth decreased below the spin-reorientation transition ($T \simeq 150$ K) and reached $m_z \simeq 2.3\,\mu_B$ at 0 K. m_z(Fe) and m_{xy}(Fe) were almost the same for the two magnets, except $T < T_R \simeq 150$ K. m_z(Fe) and m_{xy}(Fe) in $Nd_2Fe_{14}B$ exhibited a large reduction and increment, respectively, below $T \simeq 150$ K, and this dependence was reflected in total magnetizations M_z and M_{xy} in $Nd_2Fe_{14}B$. The contributions of the increasing function of T,

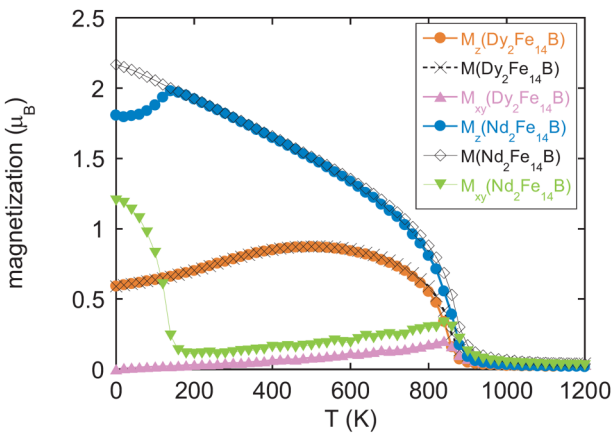

FIG. 2. Temperature dependences of M_z, M, and M_{xy} at the zero field for $Dy_2Fe_{14}B$ and $Nd_2Fe_{14}B$.

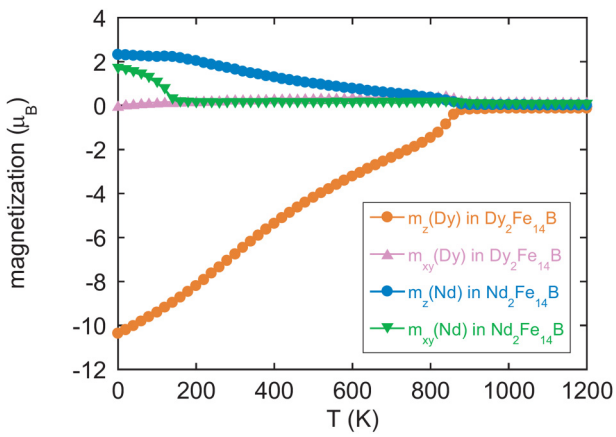

FIG. 3. Temperature dependences of m_z(Dy) and m_{xy}(Dy) in $Dy_2Fe_{14}B$, and m_z(Nd) and m_{xy}(Nd) in $Nd_2Fe_{14}B$ at the zero field.

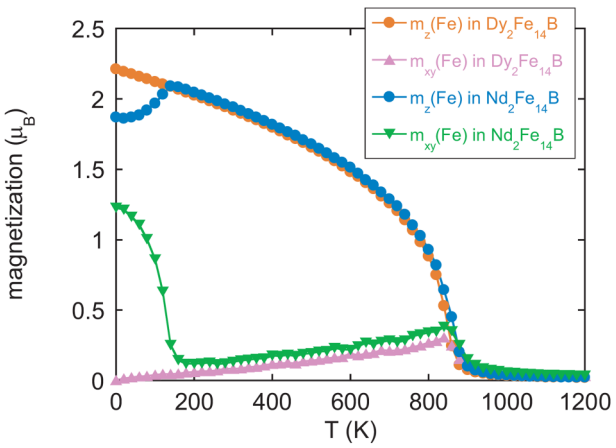

FIG. 4. Temperature dependences of m_z(Fe) and m_{xy}(Fe) in $Dy_2Fe_{14}B$, and m_z(Fe) and m_{xy}(Fe) in $Nd_2Fe_{14}B$ at the zero field.

that is, m_z(Dy), and the decreasing function of T, that is, m_z(Fe), exhibited M_z in $Dy_2Fe_{14}B$ with a peak around $T = 0.58T_c$.

Subsequently, we studied the field dependences of the magnetizations in $Dy_2Fe_{14}B$ and $Nd_2Fe_{14}B$. We focused on the magnetizations at the temperature $T = 0.46T_c$, close to room temperature. In Figs. 5(a) and 5(b), we depict h_x and h_z dependences of M_x, M_z, and M in $Dy_2Fe_{14}B$ and $Nd_2Fe_{14}B$, respectively. In $Dy_2Fe_{14}B$, M_x increased linearly up to $h_x \simeq 18.0$ T. Around $h_x \simeq 18.0$ T, the rate of increase of M_x changed and became slowly for $h_x > 18.0$ T, while M_z decreased showing a upward convex curve to $h_x \simeq 21.0$ T.

In the experiments,[15,16] M_z vs h_z and M_x vs h_x were observed less than 1.5 T (up to around 1.0 T), and the field of a crossing point of extensions of these lines was determined as the anisotropy field of $Dy_2Fe_{14}B$, which was $h_A \simeq 15.0$ T at room temperature (300 K). There M_z was almost saturated for $h_z < 1.5$ T and considered to be a saturated magnetization, i.e., $M_z = M_{sat} = 0.824\mu_B$/site. In the simulation, M_z gradually increases for h_z [Fig. 5(a)]. However, we adopted the same procedure as the experiments to estimate h_A in the simulation. The saturated M_z was determined as $M_z = 0.85\,\mu_B$/site at $h_z = 1.0$ T, and h_A was estimated as the field of the crossing point of the line of M_x vs h_x and line of $M_z = 0.85\,\mu_B$/site. Then we found $h_A \simeq 15.0$ T which corresponds to the experimental estimation. We give a discussion about an alternative estimation later.

On the other hand, h_A is clearly determined in $Nd_2Fe_{14}B$ in the same way as the experiment.[15,16] In Fig. 5(b), M_z was almost constant and M_x increased linearly up to $h_x \simeq 6.0$ T, above which M_x remained constant (fully saturated). This is in agreement with experimentally estimated values, $h_A \simeq 6.7$ T[15,16] at room temperature (300 K).

It was observed that the simulation approximately reproduced the field dependencies of the magnetizations in both $Dy_2Fe_{14}B$ and $Nd_2Fe_{14}B$, and that $Dy_2Fe_{14}B$ had a much larger anisotropy field than $Nd_2Fe_{14}B$.

In this study, we estimated the anisotropy energy K_1 using the following relation:

$$K_1 = \frac{1}{2} h_A M_{sat}, \tag{16}$$

where M_{sat} is the saturation magnetization. In the experiments,[16] $M_{sat} = 0.824\mu_B$/site and $h_A \simeq 15.0$ T at room temperature (300 K) yielded $K_1 \simeq 4.22\,\mathrm{MJ/m^3}$. In the simulation, we used $M_{sat} = M_z$ at $h_z = 1.0$ T, i.e., $M_{sat} = M_z = 0.85\mu_B$/site, and thus we obtained $K_1 \simeq 4.35\,\mathrm{MJ/m^3}$ with $h_A = 15.0$ T. We found that the obtained K_1 corresponds to the experimental K_1. However, considering that M_x as a function of h_x and M_z as a function of h_z gradually increase at larger fields, it is difficult to estimate K_1 precisely. We discuss this point later.

In contrast, in $Nd_2Fe_{14}B$, M_x increased linearly up to $h_x \simeq 6.0$ T, above which M_x became saturated. We considered

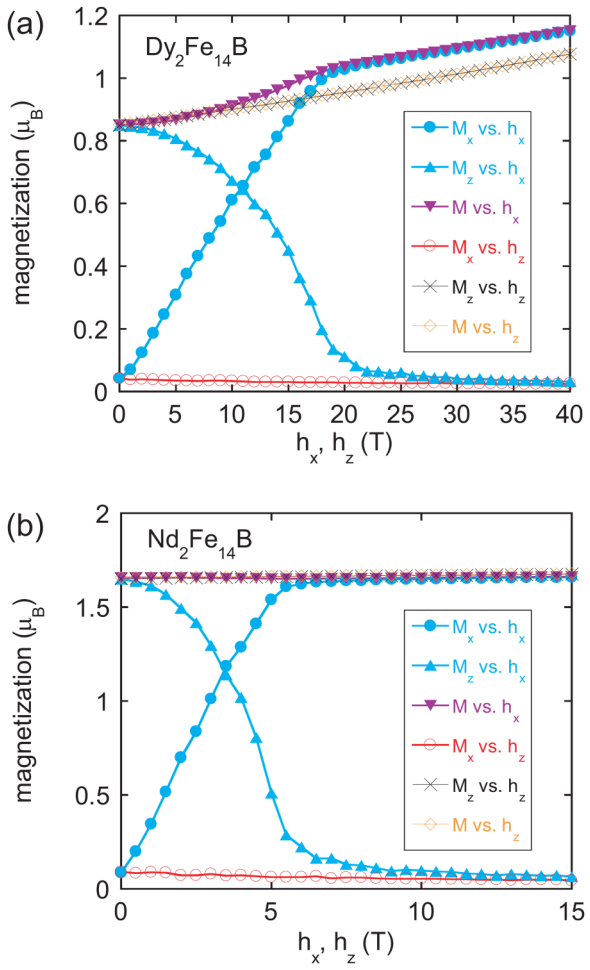

FIG. 5. h_x and h_z dependences of M_x, M_z, and M in (a) $Dy_2Fe_{14}B$ and (b) $Nd_2Fe_{14}B$. $T = 0.46T_c$.

TABLE I. Estimated values of h_A, M_{sat}, and K_1 at $T = 0.46T_c$ in comparison with experimental data at room temperature. See text for values in square brackets.

$R_2Fe_{14}B$	h_A (T)	M_{sat} (μ_B/site)	K_1 (MJ/m^3)
$Dy_2Fe_{14}B$ (simulation)	15.0 [21.0]	0.85 [0.96]	4.35 [6.88]
(experiment)	15.0	0.824	4.22
$Nd_2Fe_{14}B$ (simulation)	6.0	1.65	3.31
(experiment)	6.7	1.91	4.27

$M_z = 1.65\,\mu_B$/site at $h_z = 1.0$ T as M_{sat}. Using $h_A = 6.0$ T, we obtained $K_1 = 3.31$ MJ/m^3. In the experiments, $M_{sat} = 1.91\,\mu_B$/site and $h_A = 6.7$ T were estimated at room temperature (300 K),[16] which yielded $K_1 \simeq 4.27$ MJ/m^3. The estimated h_A, M_{sat}, and h_A are summarized in Table I.

To investigate the field dependences of the magnetizations of the constituent atoms, we give in Figs. 6(a) and 6(b), h_x dependences of m_z(Dy), m_x(Dy), and m(Dy) for low and high fields, respectively. In Fig. 6(c), we show h_x dependences of m_z(Fe), m_x(Fe), and m(Fe) on $Dy_2Fe_{14}B$.

We also present in Figs. 7(a) and 7(b), h_x dependences of m_z(Nd), m_x(Nd), and m(Nd) and h_x dependences of m_z(Fe), m_x(Fe), and m(Fe) on $Nd_2Fe_{14}B$, respectively. Magnetization m_x(Dy) increased in the negative direction up to $h_x = 18$ T at a constant rate and then reduced above $h_x = 18$ T at a slower rate. Magnetization m_x(Dy) became zero around $h_x = 98$ T and increased linearly in the positive direction at larger fields. It is worth noting that m(Dy) decreased the upward convexity to $h_x = 18$ T, then linearly to $h_x = 98$ T, reached m(Dy)$\simeq 0$ at $h_x = 98$ T, and increased linearly above $h_x = 98$ T. This indicates that a paramagnetic-like state of the Dy moments was realized around $h_x = 98$ T. With respect to the Fe moment, m_x(Fe) increased linearly and m_z(Fe) decreased with an upward convex curve up to 18 T, above which m_x(Fe) became saturated. On the other hand, m_x(Nd) and m_x(Fe) in $Nd_2Fe_{14}B$ increased linearly up to $h_x = 6.0$ T and became saturated around $M_x \simeq M \simeq 1.25\,\mu_B$/site and $M_x \simeq M \simeq 1.83\,\mu_B$/site, respectively. From zero to 6.0 T, m(Nd) was slightly reduced, whereas m(Fe) remained constant. In Figs. 8(a) and 8(b), we depict alignments of the (averaged) moments of the Dy and Fe atoms in $Dy_2Fe_{14}B$ and those of the Nd and Fe atoms in $Nd_2Fe_{14}B$, respectively, as functions of h_x.

We noticed that the Dy and Fe moments did not yet become antiparallel and parallel, respectively, to the x-axis at $h_x = 18.0$ T, but they got antiparallel and parallel over $h_x = 21.0$ T, where M_z as a function of h_x was nearly zero [Fig. 5(a)]. In that sense, $h_x = 21.0$ T is a critical value and may be adopted as h_A. When $h_A = 21.0$ T was adopted, $M_{sat} = M_z = 0.96\,\mu_B$/site at $h_z = 21.0$ T, which yielded $K_1 \simeq 6.88$ MJ/m^3. These values for h_A, M_{sat}, and K_1 were also given by square brackets for reference in Table I.

We compared our results with mean-field studies. Radwański and Franse studied magnetic properties of $R_2Fe_{14}B$ using a simple two-sublattice (moments of R and Fe) mean-field theory.[30] They estimated the anisotropy constant of K_1 treating only B_0^0 for $B_l^m(=\Theta_l A_l^m \langle r^l \rangle)$ for the crystal electric field energy of rare earth atoms. They gave $K_1 = 21$ MJ/m^3 at 300 K for $Dy_2Fe_{14}B$. This value is too large compared with the experimental value and our

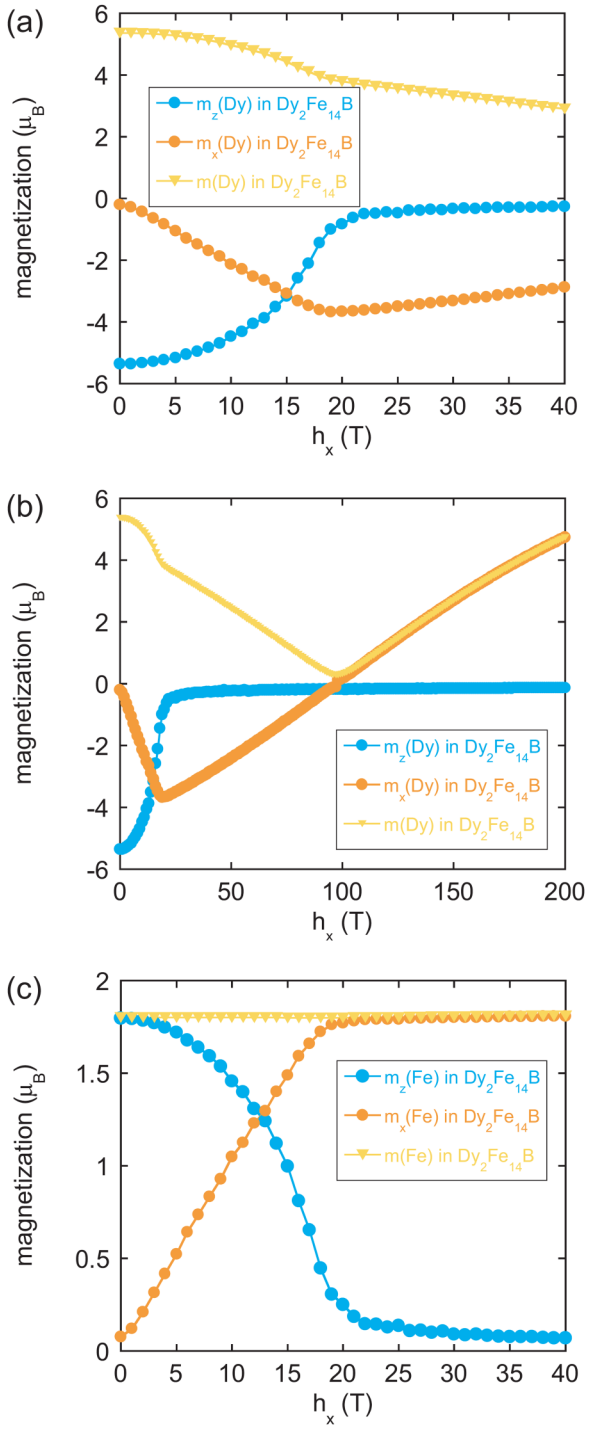

FIG. 6. h_x dependences of m_z(Dy), m_x(Dy), and m(Dy) in $Dy_2Fe_{14}B$ in (a) a low field range and (b) in a wider field range. h_x dependences of (c) m_z(Fe), m_x(Fe), and m(Fe) in $Dy_2Fe_{14}B$. $T = 0.46T_c$.

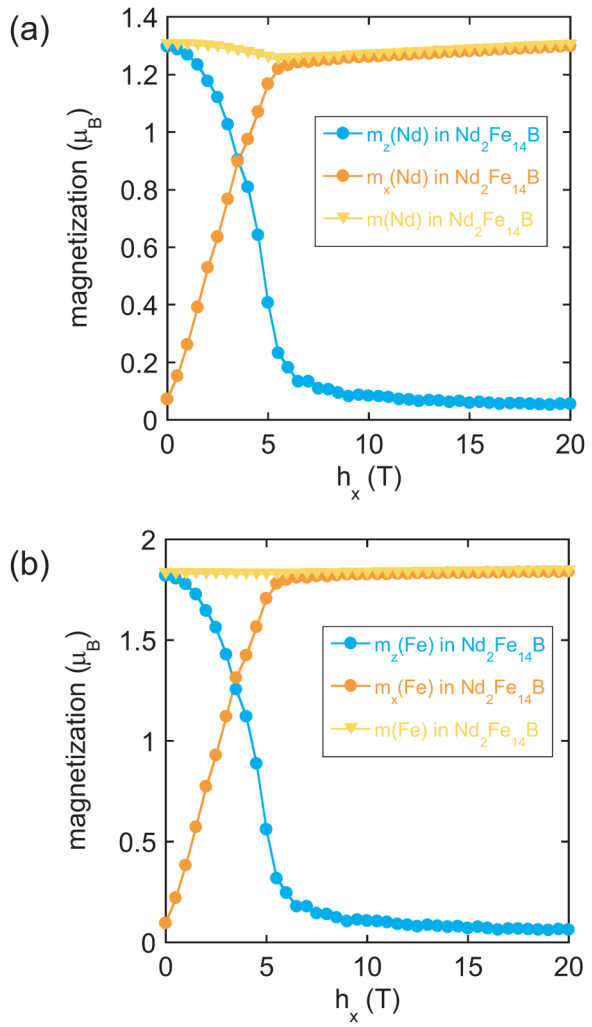

FIG. 7. h_x dependences of (a) m_z(Nd), m_x(Nd), and m(Nd) and (b) m_z(Fe), m_x(Fe), and m(Fe) in $Nd_2Fe_{14}B$. $T = 0.46T_c$.

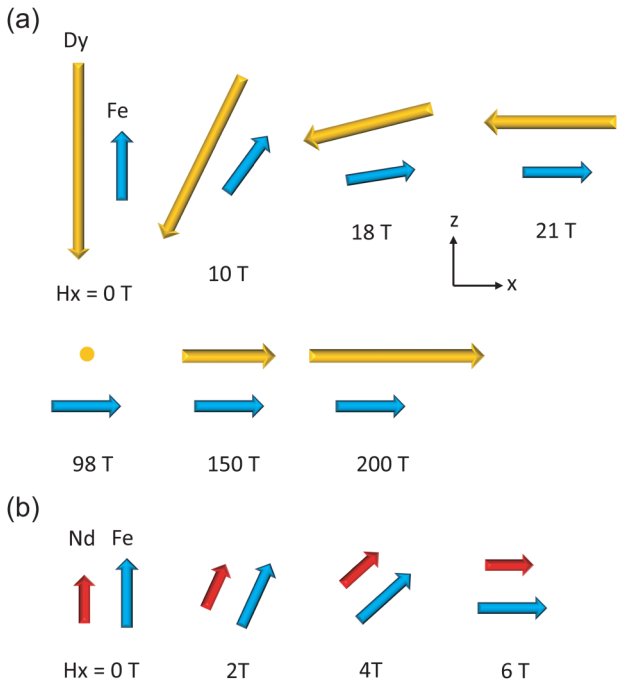

FIG. 8. Alignments of (a) Dy and Fe moments in $Dy_2Fe_{14}B$ and (b) Nd and Fe moments in $Nd_2Fe_{14}B$ as a function of h_x. $T = 0.46T_c$.

estimation. This may be due to the ignorance of higher order of B_l^m and thermal fluctuation effects, which are adequately treated in the atomistic model approach besides the difference in modeling.

Ito *et al.* also performed a simple two-sublattice mean-field study of the magnetic properties, treating B_0^0, B_0^2, and B_0^4.[31] They showed under an applied field parallel to the hard axis (x direction) a small noncollinearity of Nd and Fe moments in $Nd_2Fe_{14}B$ at room temperature and a non collinearity of Dy and Fe moments in $Dy_2Fe_{14}B$ at a low temperature. Miura *et al.* studied the magneto-crystalline anisotropy in $R_2Fe_{14}B$ in relation to non-collinearity effect and showed that angular difference between the total and Fe moments in $Nd_2Fe_{14}B$ is very small in the whole temperature region, while a big angular difference exists in $Dy_2Fe_{14}B$ especially at low temperatures.[57]

We show in Fig. 8 that the average Nd and Fe moments have collinearity at room temperature, which is close to Miura's result. Our result also presented that the average Dy and Fe moments have a slight non collinearity at room temperature in the field dependence. This indicates that collinearity in $Dy_2Fe_{14}B$ may become stronger at higher temperatures in the field dependence, in which temperature and thermal fluctuation effect may play an important role.

B. Effect of Dy random substitution on magnetization reversal in the Nd magnet

In this subsection, we discuss the effects of Dy random substitution on the coercivity enhancement of Nd magnets. Because the modification of the (001) interface is more efficient for coercivity enhancement than that of the (100) interface,[49] we focus on the (001) surface in the present work. We considered two types of systems. In system I, the (001) surface [top ($n = 1$) and bottom ($n = 19$)] layers were in contact with vacuum [Fig. 9(a)], whereas in system II, the surface layers were in contact with a soft magnet (grain boundary) phase [Fig. 9(b)]. The layers of Nd atoms in the hard magnet are numbered as $n = 1, 2, \ldots$ in Figs. 9(a) and 9(b). We used open and periodic boundary conditions in systems I and II, respectively, along the c axis and periodic boundary conditions along the a and b axes in both systems. The hard (soft) magnet part comprised $12 \times 12 \times 9$ ($12 \times 12 \times 3$) unit cells along the a, b, and c axes.

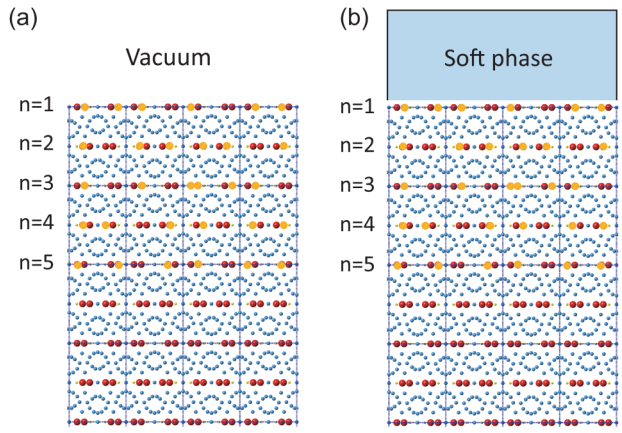

FIG. 9. (a) System I. The Nd surface layers are in contact with vacuum. (b) System II. The Nd surface layers are in contact with a soft magnet phase of three-unit-cell thickness. The Nd layers are numbered as $n = 1, 2, \ldots$. Nd (red) sites are replaced randomly by Dy atoms (orange) with concentration P between $n = 1$ and $n = 5$ and between $n = 15$ and $n = 19$.

The structure of the grain boundary phase was complicated in the experiments, and several amorphous-like structures, depending on the experimental conditions, were suggested. It was difficult to theoretically estimate the microscopic parameters of the grain-boundary phase, and microscopic magnetic parameters are not currently available. Only few first-principles studies on amorphous-like structures have been conducted.[58,59] We employed the same crystal structure in the soft magnet phase as in the hard magnet phase but adopted smaller magnetic parameters, as has been applied in micromagnetic simulations for Nd magnets. The values of all exchange interactions (anisotropy energies) inside the soft magnet phase were set to half (one-fifth) of those in the hard magnet phase. With this modeling, it is possible to catch important features of the effect of the soft magnet phase.

In our previous study,[50] all Nd atoms from the first to the nth layer were substituted with Dy atoms, and n dependence of the threshold field was investigated. In this study, Nd atoms were randomly substituted by Dy atoms with concentration P in the Nd layers between $n = 1$ and $n = 5$ (between $n = 15$ and $n = 19$) in systems I and II [Figs. 9(a) and 9(b)], and P dependence of the threshold field was investigated.

In Fig. 10, P dependences of the threshold fields at $T = 0.46T_c$ for systems I and II are illustrated. The value (percentage) of each symbol in the figure indicates the ratio of the threshold field to that of $P = 0$. We observed that the threshold fields increased almost linearly with P. The slope of the increase in the threshold field in system II was nearly identical to that in system I. In Ref. 50, we observed that n dependence of the threshold fields was approximately linear increase and the slope of the increment was nearly identical in both systems. This suggests that the layer-by-layer substitution and random substitution caused no significant difference.

When the concentration of Dy atoms was higher, the nucleation feature changed from surface nucleation to bulk nucleation, as in the case of n dependence of the threshold field in Ref. 50. We analyzed the critical value of P to distinguish between the surface and bulk nucleation. In Fig. 11, the ratios between the surface and bulk nucleation at the threshold fields are given as functions of P in systems I and II at $T = 0.46T_c$. We estimated the ratios from six samples of reversal at each P in each system. We found that a larger concentration (larger P) was necessary to realize the bulk

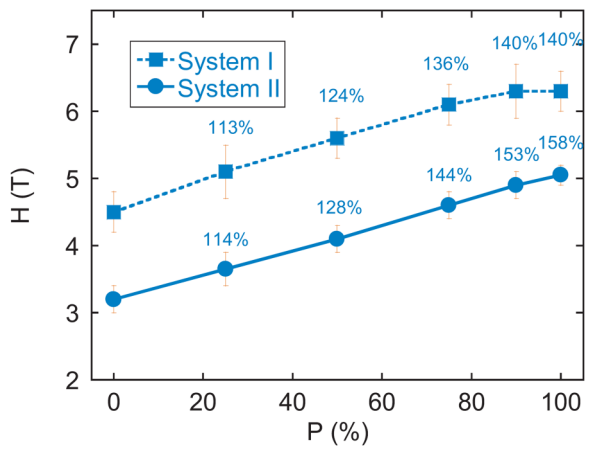

FIG. 10. P dependences of the threshold fields at $T = 0.46T_c$ for systems I (dashed line with squares) and II (solid line with circles).

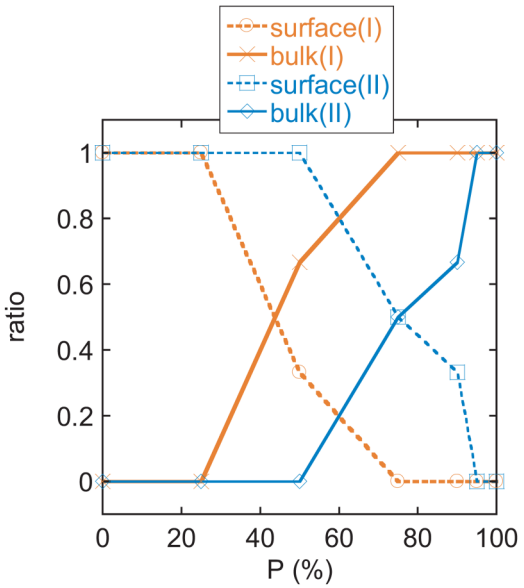

FIG. 11. P dependences of the ratio between the surface and bulk nucleation at $T = 0.46T_c$ for systems I (dashed line with squares) and II (solid line with circles).

nucleation in system II than in system I, because a domain wall generated in the soft magnet phase caused a surface nucleation more easily. The critical P in system I was $P_c \simeq 40\%$ and that in system II was $P_c \simeq 75\%$.

In the study of n dependence, the critical n between the surface and bulk nucleation was $n_c \simeq 1.5$ for a system in contact with vacuum and $n_c \simeq 3$ for a system in contact with a soft magnet phase, corresponding to 30% and 60% Dy substitution between $n = 1$ and $n = 5$, respectively. Thus, the Dy substitution ratio for bulk nucleation was larger for random substitution than for layer-by-layer substitution. However, the enhancement effect against the Dy substitution ratio was almost the same for the layer-by-layer and random substitutions.

These observations suggest that in Dy substitution near the surface of the hard magnetic phase, the arrangement of Dy atoms is not very important, but the concentration density of Dy atoms is significant for the enhancement of the coercivity of the Nd magnet, and Dy substitution enhances the coercive force with a ratio proportional to the density of Dy atoms.

We compared our observation with a micromagnetics model study.[26] Bance *et al.* studied a micromagnetics model (50 nm) consisting of $Nd_2Fe_{14}B$ core, 4-nm $(Dy_{47},Nd_{53})_2Fe_{14}B$ shell, and a 2-nm soft surface defect.[26] They showed that the coercive force was enhanced from 3.23 to 4.97 T at 300 K. This suggest 54% increase of the coercive force with 47% Dy concentration for $n = 1$ to $n \simeq 7$. In Fig. 10, the coercive force was enhanced from 3.10 to 4.10 T at $0.46T_c$ indicating that 28% increase with 50% concentration for $n = 1$ to $n = 5$. We confirmed a similar tendency of coercivity enhancement between the two approaches (micromagnetic and atomistic simulations), but found that the increase ratio of the coercivity in our results is smaller than that of the micromagnetic simulations. This may be due to the inclusion of thermal fluctuation effects in the evaluation.

V. SUMMARY

To understand the Dy substitution effect in neodymium magnets, it is important to determine the differences in thermodynamic properties between $Dy_2Fe_{14}B$ and $Nd_2Fe_{14}B$. In this paper, we first investigated these differences using an atomistic model. Applying the Metropolis importance-sampling Monte Carlo (MC) method, we presented the temperature dependences of the magnetizations of the magnets and their components at zero field. The simulated temperature-magnetization curve (M_z) of $Dy_2Fe_{14}B$ exhibited characteristic features of the experimentally observed ones: M_z increased by lowering the temperature from T_c, showed a peak at a high temperature, and slowly decreased to zero temperature. This was found to originate from the Fe positive magnetization (m_z) showing an upward convex dependence with a large curvature below T_c and the Dy negative magnetization (m_z) showing a downward-upward-downward convex dependence with low curvatures. On the other hand, the temperature dependence of M_z on $Nd_2Fe_{14}B$ was mainly reflected by m_z of the Fe moments. Although the origin of the spin reorientation (SR) is the property of the CEF potential of Nd atoms, m_z of Fe moments was more reduced under $T = T_R$ than that of Nd atoms.

The estimated value of the magnetization (M_z) of $Dy_2Fe_{14}B$ at zero temperature agreed with the experimentally observed ones, and M_z at the peak position for $Dy_2Fe_{14}B$ was also found to be an approximation of the experimentally observed ones as well as a good approximation of the peak magnetization at the spin-reorientation transition temperature in $Nd_2Fe_{14}B$. We also found that the critical temperatures of the two magnets were very close, which was consistent with the experimental results, although the critical temperatures were a little overestimated. This overestimation was mainly due to an overestimation of the exchange interactions (Fe–Fe and Fe–R).

The magnetization profile (m_z, m_{xy} at zero field) of Fe atoms in $Dy_2Fe_{14}B$ was similar to that in $Nd_2Fe_{14}B$, except at temperatures below the SR transition temperature of $Nd_2Fe_{14}B$, which suggests that Fe moments are hardly affected by replacement of Nd by Dy under zero field.

We also studied the field dependences of the magnetizations of the two magnets and their components. In $Dy_2Fe_{14}B$, M_x as a function of h_x increased linearly up to around 18 T and then gradually increased at higher fields. This situation makes an accurate estimation of the anisotropy field h_A difficult. When the experimental procedure was followed in the simulation, the estimation corresponded to the experimental one: $h_A = 15.0$ T. We also estimated h_A with a different definition, in which the Dy and Fe moments were antiparallel and parallel to the x axis (hard axis), respectively, and obtained $h_A = 21.0$ T. With increasing h_x, the Dy and Fe moments were rotated slightly tilting from the antiparallel configuration before 21.0 T. At higher h_x, the Dy moment decreased ($m_x < 0$) and increased ($m_x > 0$) through a paramagnetic-like state $m_x \simeq 0$ at $h_x \simeq 98$ T. On the other hand, in $Nd_2Fe_{14}B$, the Nd and Fe moments maintained collinearity (parallel configuration) under the field change of h_x, and h_A was estimated to be 6.0 T close to the experimental estimation: 6.7 T. We showed that $Dy_2Fe_{14}B$ had much higher h_A than $Nd_2Fe_{14}B$, as observed in the experiments.

We estimated the anisotropy energy K_1 of $Dy_2Fe_{14}B$ and $Nd_2Fe_{14}B$ from the obtained anisotropy fields (h_A) and saturated magnetizations (M_{sat}). When the experimental procedure was followed in the simulation, $K_1 = 4.35\,MJ/m^3$ was obtained, which was close to the experimentally observed value $K_1 = 4.22\,MJ/m^3$. However, using $h_A = 21.0$ T, $K_1 = 6.88\,MJ/m^3$ was yielded. In $Nd_2Fe_{14}B$, $K_1 = 3.31\,MJ/m^3$ was obtained, which is an approximation of the experimentally observed one: $4.27\,MJ/m^3$.

Subsequently, we investigated the effect of Dy random substitution in a range close to the grain surface on the magnetization reversal in the neodymium permanent magnet. We studied two systems: system I whose surface layers were in contact with vacuum and system II whose surface layers were in contact with a soft magnet (grain boundary). The threshold fields increased almost linearly with the concentration of Dy atoms, and the slopes of the increments of the threshold fields in systems I and II were nearly identical. These results are similar to those obtained for n (layer number) dependences of the threshold fields in the layer-by-layer substitution studied in Ref. 50, although the critical density between the surface and bulk nucleation was different. This indicates that if the Dy substitution is limited to the range close to the grain surface, the arrangement of Dy atoms is not so important,

but the concentration density of Dy atoms is significant for the enhancement of the coercivity of the Nd magnet.

ACKNOWLEDGMENTS

The authors would like to thank Dr. Hirosawa for instructive discussions on the experimental results for $R_2Fe_{14}B$, Professor Akai for helpful discussions on the magnetic parameters for $Dy_2Fe_{14}B$ using the KKR first-principles method, and Dr. Toga for useful discussions on the properties of Nd magnets. This work was supported by World Premier International Research Center Initiative (WPI), MEXT, Japan, and partially supported by Grants-in-Aid for Scientific Research B (No. 24K01332) from MEXT. Numerical calculations were performed using the Numerical Materials Simulator at the National Institute for Materials Science.

AUTHOR DECLARATIONS

Conflict of Interest

The authors have no conflicts to disclose.

Author Contributions

Masamichi Nishino: Conceptualization (lead); Data curation (equal); Formal analysis (lead); Funding acquisition (equal); Investigation (lead); Methodology (equal). **Hiroshi Hayasaka:** Data curation (equal); Formal analysis (equal); Investigation (equal). **Seiji Miyashita:** Conceptualization (equal); Formal analysis (equal); Funding acquisition (equal); Investigation (equal).

DATA AVAILABILITY

The data that support the findings of this study are available from the corresponding author upon reasonable request.

REFERENCES

[1]R. Friedberg and D. I. Paul, "New theory of coercive force of ferromagnetic materials," Phys. Rev. Lett. **34**, 1234–1237 (1975).
[2]A. Sakuma, S. Tanigawa, and M. Tokunaga, "Micromagnetic studies of inhomogeneous nucleation in hard magnets," J. Magn. Magn. Mater. **84**, 52–58 (1990).
[3]A. Sakuma, "The theory of inhomogeneous nucleation in uniaxial ferromagnets," J. Magn. Magn. Mater. **88**, 369–375 (1990).
[4]S. Mohakud, S. Andraus, M. Nishino, A. Sakuma, and S. Miyashita, "Temperature dependence of the threshold magnetic field for nucleation and domain wall propagation in an inhomogeneous structure with grain boundary," Phys. Rev. B **94**, 054430 (2016).
[5]S. Hirosawa, M. Nishino, and S. Miyashita, "Perspectives for high-performance permanent magnets: Applications, coercivity, and new materials," Adv. Nat. Sci.: Nanosci. Nanotechnol. **8**, 013002 (2017).
[6]A. L. Wysocki and V. P. Antropov, "Micromagnetic simulations with periodic boundary conditions: Hard-soft nanocomposites," J. Magn. Magn. Mater. **428**, 274–286 (2017).
[7]I. E. Uysal, M. Nishino, and S. Miyashita, "Magnetic field threshold for nucleation and depinning of domain walls in the neodymium permanent magnet $Nd_2Fe_{14}B$," Phys. Rev. B **101**, 094421 (2020).
[8]S. Okamoto, R. Goto, N. Kikuchi, O. Kitakami, T. Akiya, H. Sepehri-Amin, T. Ohkubo, K. Hono, K. Hioki, and A. Hattori, "Temperature-dependent magnetization reversal process and coercivity mechanism in Nd-Fe-B hot-deformed magnets," J. Appl. Phys. **118**, 223903 (2015).
[9]T. Pramanik, A. Roy, R. Dey, A. Rai, S. Guchhait, H. C. Movva, C.-C. Hsieh, and S. K. Banerjee, "Angular dependence of magnetization reversal in epitaxial chromium telluride thin films with perpendicular magnetic anisotropy," J. Magn. Magn. Mater. **437**, 72–77 (2017).
[10]M. Sagawa and S. Hirosawa, "Magnetic hardening mechanism in sintered *R*–Fe–B permanent magnets," J. Mater. Res. **3**, 45–54 (1988).
[11]J. F. Herbst, J. J. Croat, F. E. Pinkerton, and W. B. Yelon, "Relationships between crystal structure and magnetic properties in $Nd_2Fe_{14}B$," Phys. Rev. B **29**, 4176–4178 (1984).
[12]S. Hirosawa, Y. Matsuura, H. Yamamoto, S. Fujimura, M. Sagawa, and H. Yamauchi, "Single crystal measurements of anisotropy constants of $R_2Fe_{14}B$ (R=Y, Ce, Pr, Nd, Gd, Tb, Dy and Ho)," Jpn. J. Appl. Phys. **24**, L803–L805 (1985).
[13]A. V. Andreev, A. V. Deriagin, N. V. Kudrevatykh, N. V. Mushnikov, and V. A. Reimer, "The magnetism of $Y_2Fe_{14}B$ and $Nd_2Fe_{14}B$ and their hydrides," Zh. Eksperimentalnoi Teor. Fiz. **90**, 1042–1050 (1986).
[14]H. Kronmüller, K.-D. Durst, and M. Sagawa, "Analysis of the magnetic hardening mechanism in RE-FeB permanent magnets," J. Magn. Magn. Mater. **74**, 291–302 (1988).
[15]J. F. Herbst, "$R_2Fe_{14}B$ materials: Intrinsic properties and technological aspects," Rev. Mod. Phys. **63**, 819–898 (1991).
[16]S. Hirosawa, Y. Matsuura, H. Yamamoto, S. Fujimura, M. Sagawa, and H. Yamauchi, "Magnetization and magnetic anisotropy of $R_2Fe_{14}B$ measured on single crystals," J. Appl. Phys. **59**, 873–879 (1986).
[17]O. Yamada, Y. Ohtsu, F. Ono, M. Sagawa, and S. Hirosawa, "Magnetocrystalline anisotropy in $Nd_2Fe_{14}B$ intermetallic compound," J. Magn. Magn. Mater. **70**, 322–324 (1987).
[18]N. V. Mushnikov, P. B. Terent'ev, and E. V. Rosenfel'd, "Magnetic anisotropy of the $Nd_2Fe_{14}B$ compound and its hydride $Nd_2Fe_{14}BH_4$," Phys. Metals Metallogr. **103**, 39–50 (2007).
[19]T. Kohashi, K. Motai, T. Nishiuchi, and S. Hirosawa, "Magnetism in grain-boundary phase of a NdFeB sintered magnet studied by spin-polarized scanning electron microscopy," Appl. Phys. Lett. **104**, 232408 (2014).
[20]S. Sugimoto, "Current status and recent topics of rare-earth permanent magnets," J. Phys. D: Appl. Phys. **44**, 064001 (2011).
[21]K. Hirota, H. Nakamura, T. Minowa, and M. Honshima, "Coercivity enhancement by the grain boundary diffusion process to Nd-Fe-B sintered magnets," IEEE Trans. Magn. **42**, 2909–2911 (2006).
[22]F. Xu, J. Wang, X. Dong, L. Zhang, and J. Wu, "Grain boundary microstructure in DyF3-diffusion processed Nd-Fe-B sintered magnets," J. Alloys Compd. **509**, 7909–7914 (2011).
[23]K. Löewe, C. Brombacher, M. Katter, and O. Gutfleisch, "Temperature-dependent Dy diffusion processes in Nd-Fe-B permanent magnets," Acta Mater. **83**, 248–255 (2015).
[24]W. Chen, J. M. Luo, Y. W. Guan, Y. L. Huang, M. Chen, and Y. H. Hou, "Grain boundary diffusion of Dy films prepared by magnetron sputtering for sintered Nd–Fe–B magnets," J. Phys. D: Appl. Phys. **51**, 185001 (2018).
[25]T.-H. Kim, T. Sasaki, T. Ohkubo, Y. Takada, A. Kato, Y. Kaneko, and K. Hono, "Microstructure and coercivity of grain boundary diffusion processed Dy-free and Dy-containing Nd–Fe–B sintered magnets," Acta Mater. **172**, 139–149 (2019).
[26]S. Bance, J. Fischbacher, A. Kovacs, H. Oezelt, F. Reichel, and T. Schrefl, "Thermal activation in permanent magnets," JOM **67**, 1350–1356 (2015).
[27]J. Fischbacher, A. Kovacs, L. Exl, J. Kühnel, E. Mehofer, H. Sepehri-Amin, T. Ohkubo, K. Hono, and T. Schrefl, "Searching the weakest link: Demagnetizing fields and magnetization reversal in permanent magnets," Scr. Mater. **154**, 253–258 (2018).
[28]H. Kronmüller and M. Fähnle, *Micromagnetism and the Microstructure of Ferromagnetic Solids*, Cambridge Studies in Magnetism (Cambridge University Press, 2003).
[29]G. Grinstein and R. H. Koch, "Coarse graining in micromagnetics," Phys. Rev. Lett. **90**, 207201 (2003).
[30]R. J. Radwański and J. J. M. Franse, "Rare-earth contribution to the magnetocrystalline anisotropy energy in $R_2Fe_{14}B$," Phys. Rev. B **36**, 8616–8621 (1987).

[31]M. Ito, M. Yano, N. M. Dempsey, and D. Givord, "Calculations of the magnetic properties of $R_2M_{14}B$ intermetallic compounds (R=rare earth, M=Fe, Co)," J. Magn. Magn. Mater. **400**, 379–383 (2016).
[32]P. Peczak, A. M. Ferrenberg, and D. P. Landau, "High-accuracy Monte Carlo study of the three-dimensional classical Heisenberg ferromagnet," Phys. Rev. B **43**, 6087–6093 (1991).
[33]J. L. García-Palacios and F. J. Lázaro, "Langevin-dynamics study of the dynamical properties of small magnetic particles," Phys. Rev. B **58**, 14937–14958 (1998).
[34]M. Nishino and S. Miyashita, "Realization of the thermal equilibrium in inhomogeneous magnetic systems by the Landau-Lifshitz-Gilbert equation with stochastic noise, and its dynamical aspects," Phys. Rev. B **91**, 134411 (2015).
[35]Y. Toga, M. Matsumoto, S. Miyashita, H. Akai, S. Doi, T. Miyake, and A. Sakuma, "Monte Carlo analysis for finite-temperature magnetism of $Nd_2Fe_{14}B$ permanent magnet," Phys. Rev. B **94**, 174433 (2016).
[36]M. Nishino, Y. Toga, S. Miyashita, H. Akai, A. Sakuma, and S. Hirosawa, "Atomistic-model study of temperature-dependent domain walls in the neodymium permanent magnet $Nd_2Fe_{14}B$," Phys. Rev. B **95**, 094429 (2017).
[37]T. Hinokihara, M. Nishino, Y. Toga, and S. Miyashita, "Exploration of the effects of dipole-dipole interactions in $Nd_2Fe_{14}B$ thin films based on a stochastic cutoff method with a novel efficient algorithm," Phys. Rev. B **97**, 104427 (2018).
[38]S. Miyashita, M. Nishino, Y. Toga, T. Hinokihara, T. Miyake, S. Hirosawa, and A. Sakuma, "Perspectives of stochastic micromagnetism of $Nd_2Fe_{14}B$ and computation of thermally activated reversal process," Scr. Mater. **154**, 259–265 (2018).
[39]Y. Toga, M. Nishino, S. Miyashita, T. Miyake, and A. Sakuma, "Anisotropy of exchange stiffness based on atomic-scale magnetic properties in the rare-earth permanent magnet $Nd_2Fe_{14}B$," Phys. Rev. B **98**, 054418 (2018).
[40]M. Nishino and S. Miyashita, "Nontrivial temperature dependence of ferromagnetic resonance frequency for spin reorientation transitions," Phys. Rev. B **100**, 020403 (2019).
[41]Y. Toga, S. Miyashita, A. Sakuma, and T. Miyake, "Role of atomic-scale thermal fluctuations in the coercivity," npj Comput. Mater. **6**, 67 (2020).
[42]M. Nishino, I. E. Uysal, T. Hinokihara, and S. Miyashita, "Dynamical aspects of magnetization reversal in the neodymium permanent magnet by a stochastic Landau-Lifshitz-Gilbert simulation at finite temperature: Real-time dynamics and quantitative estimation of coercive force," Phys. Rev. B **102**, 020413(R) (2020).
[43]S. Westmoreland, R. Evans, G. Hrkac, T. Schrefl, G. Zimanyi, M. Winklhofer, N. Sakuma, M. Yano, A. Kato, T. Shoji, A. Manabe, M. Ito, and R. Chantrell, "Multiscale model approaches to the design of advanced permanent magnets," Scr. Mater. **148**, 56–62 (2018).
[44]S. C. Westmoreland, C. Skelland, T. Shoji, M. Yano, A. Kato, M. Ito, G. Hrkac, T. Schrefl, R. F. L. Evans, and R. W. Chantrell, "Atomistic simulations of α-Fe/$Nd_2Fe_{14}B$ magnetic core/shell nanocomposites with enhanced energy product for high temperature permanent magnet applications," J. Appl. Phys. **127**, 133901 (2020).
[45]Q. Gong, M. Yi, R. F. L. Evans, B.-X. Xu, and O. Gutfleisch, "Calculating temperature-dependent properties of $Nd_2Fe_{14}B$ permanent magnets by atomistic spin model simulations," Phys. Rev. B **99**, 214409 (2019).
[46]Q. Gong, M. Yi, and B.-X. Xu, "Multiscale simulations toward calculating coercivity of Nd–Fe–B permanent magnets at high temperatures," Phys. Rev. Mater. **3**, 084406 (2019).
[47]Q. Gong, M. Yi, R. F. L. Evans, O. Gutfleisch, and B.-X. Xu, "Anisotropic exchange in Nd–Fe–B permanent magnets," Mater. Res. Lett. **8**, 89–96 (2020).
[48]S. Miyashita, M. Nishino, Y. Toga, T. Hinokihara, I. E. Uysal, T. Miyake, H. Akai, S. Hirosawa, and A. Sakuma, "Atomistic theory of thermally activated magnetization processes in $Nd_2Fe_{14}B$ permanent magnet," Sci. Technol. Adv. Mater. **22**, 658–682 (2021).
[49]M. Nishino, I. E. Uysal, and S. Miyashita, "Effect of the surface magnetic anisotropy of neodymium atoms on the coercivity in neodymium permanent magnets," Phys. Rev. B **103**, 014418 (2021).
[50]M. Nishino, H. Hayasaka, and S. Miyashita, "Microscopic origin of coercivity enhancement by dysprosium substitution into neodymium permanent magnets," Phys. Rev. B **106**, 054422 (2022).
[51]H. Hayasaka, M. Nishino, and S. Miyashita, "Microscopic study on the angular dependence of coercivity at zero and finite temperatures," Phys. Rev. B **105**, 224414 (2022).
[52]M. Nishino and S. Miyashita, "Quantitative estimation of coercive field in a ferromagnetic grain using field sweep simulation," Phys. Rev. B **107**, 184422 (2023).
[53]R. J. Elliott and K. W. H. Stevens, "The theory of magnetic resonance experiments on salts of the rare earths," Proc. R. Soc. A **218**, 553–566 (1953).
[54]Y. Miura, H. Tsuchiura, and T. Yoshioka, "Magnetocrystalline anisotropy of the Fe-sublattice in $Y_2Fe_{14}B$ systems," J. Appl. Phys. **115**, 17A765 (2014).
[55]M. Yamada, H. Kato, H. Yamamoto, and Y. Nakagawa, "Crystal-field analysis of the magnetization process in a series of $Nd_2Fe_{14}B$-type compounds," Phys. Rev. B **38**, 620–633 (1988).
[56]A. J. Freeman and R. E. Watson, "Theoretical investigation of some magnetic and spectroscopic properties of rare-earth ions," Phys. Rev. **127**, 2058–2075 (1962).
[57]D. Miura and A. Sakuma, "Non-collinearity effects on magnetocrystalline anisotropy for $R_2Fe_{14}B$ magnets," J. Phys. Soc. Jpn. **88**, 044804 (2019).
[58]Y. Tatetsu, S. Tsuneyuki, and Y. Gohda, "First-principles study of the role of Cu in improving the coercivity of Nd-Fe-B permanent magnets," Phys. Rev. Appl. **6**, 064029 (2016).
[59]Y. Gohda, Y. Tatetsu, and S. Tsuneyuki, "Electron theory on grain-boundary structures and local magnetic properties of neodymium magnets," Mater. Trans. **59**, 332–337 (2018).